RESEARCH ARTICLES

Disruption of Microtubules Post-Virus Entry Enhances Adeno-Associated Virus Vector Transduction

Ping-Jie Xiao,[1,2] Angela M. Mitchell,[1,3] Lu Huang,[4] Chengwen Li,[1] and R. Jude Samulski[1,5,*]

[1]Gene Therapy Center, [2]Cell and Developmental Biology, and Departments of [3]Microbiology and Immunology,
[4]Statistics, and [5]Pharmacology, University of North Carolina at Chapel Hill, Chapel Hill, North Carolina.

Perinuclear retention of viral particles is a poorly understood phenomenon observed during many virus infections. In this study, we investigated whether perinuclear accumulation acts as a barrier to limit recombinant adeno-associated virus (rAAV) transduction. After nocodazole treatment to disrupt microtubules at microtubule-organization center (MT-MTOC) after virus entry, we observed higher rAAV transduction. To elucidate the role of MT-MTOC in rAAV infection and study its underlying mechanisms, we demonstrated that rAAV's perinuclear localization was retained by MT-MTOC with fluorescent analysis, and enhanced rAAV transduction from MT-MTOC disruption was dependent on the rAAV capsid's nuclear import signals. Interestingly, after knocking down RhoA or inhibiting its downstream effectors (ROCK and Actin), MT-MTOC disruption failed to increase rAAV transduction or nuclear entry. These data suggest that enhancement of rAAV transduction is the result of increased trafficking to the nucleus via the RhoA-ROCK-Actin pathway. Ten-fold higher rAAV transduction was also observed by disrupting MT-MTOC in brain, liver, and tumor *in vivo*. In summary, this study indicates that virus perinuclear accumulation at MT-MTOC is a barrier-limiting parameter for effective rAAV transduction and defines a novel defense mechanism by which host cells restrain viral invasion.

INTRODUCTION

CELLS HAVE MANY STRUCTURES and machineries to protect themselves from exogenous infectious agents (e.g., viruses and bacteria).[1] For example, beside the extracellular matrix and a number of extracellular factors that can restrict infections, the plasma membrane is an important structure to limit viral infection, whereas molecularly dense cytoplasm and the nuclear envelope serve as additional barriers for viruses to reach their replication sites. As a consequence, viruses have to overcome these cellular barriers in host cells before delivering their genome to the target region for successful infection. Comprehensive knowledge about these barriers and virus–host interactions is critical in improving our understanding of basic virology and viral pathogenesis. Both strengthening these cellular barriers and weakening the viral capacity to penetrate these barriers present potentially powerful means for inhibition of viral infection. On the other hand, attenuating these barriers or designing capsid with enhanced ability to penetrate these barriers will offer promising opportunities to improve current vectors for gene therapy.

The microtubule-organization center (MTOC) is a subcellular structure at perinuclear region, from which microtubules (MTs) are nucleated to form a radial filamentous network with minus ends anchored at MTOC and plus end reaching cell surface area.[2] Because of these features, MTs and MTOC, as a trafficking center, coordinate the transport of intracellular molecules and organelles between the perinuclear region and other areas of a cell.[2] For instance, intact MTs are required for the nuclear import of several transcription factors (e.g., p53, NF-kB, pRb), and on other hand, these structures are required to sequester other proteins (e.g., c-myc, MIZ-1, smad3) in the cytoplasm to block their nuclear entry.[3–7] Numerous studies have also shown that cellular misfolded proteins are transported on MTs toward the MTOC region, where

*Correspondence: Dr. R. Jude Samulski, CB No. 7352, Gene Therapy Center, 7113 Thurston Building, The University of North Carolina at Chapel Hill, Chapel Hill, NC 27599-7352. E-mail: rjs@med.unc.edu

these misfolded proteins are then sequestered or degraded by proteasomes and lysosomes.[8,9]

Strikingly, during the early stage of infection, many incoming viruses are also delivered to and retained at a perinuclear site after entering the cells.[10–16] It has been suggested that this perinuclear site is co-localized with the MTOC region and, as observed for cellular proteins, that transport of these viruses along with MTs is facilitated by dynein motors.[9,17] Although this perinuclear retention of incoming virions seems to be a common phenomenon among many viruses, especially those that enter the nucleus, it remains unknown whether this accumulation is beneficial or inhibitory to viral infection.[9] Previous studies have shown that several viruses, including rotavirus, vaccine, and HSV, disrupt MTOC during early infection stage for reasons that have not been identified.[18–22] Despite the lack of understanding of the role of such perinuclear retention on viral infection, these observations raise an intriguing hypothesis that MTOC region serves as a subcellular barrier to restrict access of the incoming virions to their replication site (nucleus in this study) during the early stage of viral infection.

On the other hand, during late infection stage, several viruses, such as HIV, HSV, poliovirus, and norovirus, have been suggested to exploit this perinuclear accumulation to concentrate newly synthesized viral components through MTs in order to facilitate late infection events, including virion replication, assembly, or egress.[23–26] Classical virology assays usually study replication-competent viruses and measure the production of viral progeny as the readout, which is the sum of the total effects of all events in viral infection with these viruses. Given the potential involvement of MTs and MTOC throughout the entire viral infection, this method is unable to precisely dissect the perinuclear retention of incoming virions during early infection stage. Furthermore, viral replication and newly synthesized viral proteins will also confound virion distribution assays that use antibodies.[12,15]

Recombinant viruses used as gene therapy vectors (designated as viral vectors) are purposely designed to exploit only the early infection steps, including delivering and expressing viral genomes, and are deficient in late infection events, including viral replication and assembly because of the deletion of critical viral proteins.[27] As a result, these viral vectors allow researchers to more precisely separate the early infection steps from the late events, offering a promising opportunity to specifically identify the mechanisms and roles of peri-

nuclear retention on incoming virions. Adeno-associated virus (AAV) is a member in the family *Parvoviridae* and recombinant AAV (rAAV) is currently used as a gene therapy vector because of many desirable traits in gene delivery.[27] As a gene therapy vector, rAAV does not contain any viral DNA except for two inverted terminal repeats (ITR) flanking the exogenous transgene.[27] Therefore, rAAV only delivers and expresses transgenes in cells but is incapable of replicating and producing viral progeny. This attribute makes rAAV a useful model to specifically investigate virus–host interplay during the early stage of viral infection. Like many other viruses, its trafficking pathway typically starts with receptor-mediated endocytosis for cell entry, followed by cytoplasmic trafficking assisted by the endosomal routing system and MT network, and ends with nuclear entry and uncoating for successful transduction.[27–29]

In our previous study, using pharmacological agents, live-cell imaging, and flow cytometry analysis, we have demonstrated that rAAV2 exploits MTs for rapid cytoplasmic trafficking in endosomal compartments unidirectionally toward the perinuclear region and that rAAV2 transduction is reduced when the MT network is disrupted at early time point of rAAV infection.[30] In this study, we investigated the role of rAAV perinuclear retention on the effective transduction, and have further explored the detailed mechanism. A sensitive and reliable fluorescence imaging platform allowed us to examine viral trafficking in detail over time, which led us to the observation that the majority of viral particles finish cytoplasmic trafficking and localize at perinuclear region by 6–8 hr postinfection (p.i.). Manipulating host cells and viral particles using pharmacological interventions around 6–8 hr p.i. allowed us to efficiently investigate the underlying mechanism of perinuclear retention as well as the corresponding impact on viral infection.

MATERIALS AND METHODS
rAAV2 production, purification, and labeling

HEK-293 cells were used to produce rAAV2 as described previously.[31] Briefly, cells were transfected with three plasmids: pXR2 (wt or with BR mutations), pXX680, and a plasmid containing the reporter transgene (*GFP* or *Luciferase*) flanked by two ITRs. At 60 hr after transfection, cells were collected and nuclei were isolated using hypotonic buffer and Kontes homogenizer. rAAV2 particles were recovered by resuspending the nuclear pellet in PBS with 0.5% deoxycholate (DOC) and then sonicating for 1 min. Highly pure virus was then

retrieved as described previously.[32] Briefly, after DNase treatment, the virus suspension was subjected to one round of cesium chloride (CsCl) step gradient density fractionation and another round of fractionation using a continuous CsCl gradient. Determination of peak viral fractions, dialysis of virus, and measurement of viral titers by quantitative PCR (qPCR) were performed as previously described. The infectivity of AAV was determined to be approximately 1 transducing unit per 100 particles.

rAAV2 was covalently labeled with the Cy5 fluorophores as described in manufacturer's protocol with slight modification. Briefly, purified rAAV2 were incubated for 2 hr at 4°C in PBS with a 20-fold molar excess of Mono-NHS-Cy5 (GE Healthcare) over capsid protein units. Free dyes were removed from labeled viral particles by dialysis against PBS containing 5% sorbitol and viral solutions were stored at −80°C as small aliquots. Labeled viral titers were determined by both dot blot[31] and qPCR. Infectivity of the viral particles was determined by GFP reporter gene assay.

Cell culture, viral infection, and drug treatment

All cells (American Type Culture Collection) were grown in Dulbecco's modified Eagle's medium (DMEM; Invitrogen) with 10% FBS in 5% CO_2 incubator. Cells were passaged every 2–3 days for up to 10 passages, when new aliquots of frozen cells were recovered from liquid nitrogen.

For pulse infection, cells were seeded on 12 mm glass coverslips at 24 hr before infection. The next day, after incubation in DMEM containing 20 mM HEPES at 4°C for 5 min, cells were inoculated with Cy5-rAAV2 ($\sim$5,000 vgs/cell) or nonlabeled rAAV2 ($\sim$1,000–5,000 vgs/cell) at 4°C for another 40 min. Cells were then washed with PBS to remove unbound virions and transferred to a 37°C incubator (regarded as 0 hr p.i.). Pharmacological drugs were added at 6–8 hr after pulse infection unless otherwise indicated. The concentrations of drugs were 30 μM nocodazole, 25 μM colchcine, 10 μM taxol, 10 μM rhizoxin, 10 μM maytansine, 2 μM MG132, 20 μM ALLN, 10 μM H1152, and 10 μM cytochalasin D. The drugs were maintained in the culture for approximately 3 hr unless otherwise indicated.

Flow cytometry and immunofluorescence

To evaluate viral transduction, flow cytometry analysis was used to measure the mean fluorescence intensity (MFI) of GFP expression. Since slight cell toxicities from the drug treatment were observed (data not shown), to exclude the potential effect of dead cells on the viral transduction mea-

surement, we washed the cells in each well three times with PBS before harvesting for flow cytometry analysis, removing any floating or loosely attached cells. Either Trypan blue exclusion or 7-AAD exclusion assays was used to ensure cell viability over 95% for flow cytometry analysis.

For immunofluorescence, cells were washed with PBS and then fixed with 4% paraformaldehyde (PFA) for 15 min at room temperature (RT). The cells were then permeabilized with 0.2% Triton X-100 in PBS for 5 min at RT. After blocking with immunofluorescence buffer (IFB) (5% normal goat serum in PBS containing 0.05% Tween-20) for 1 hr at RT, the cells were incubated with primary antibody to detect tubulin (Ab6161; rat monoclonal from Abcam Inc.), Golgi (Ab24586; mouse monoclonal from Abcam Inc.), and/or rAAV capsid (A20 mouse monoclonal antibody) diluted in 50% IFB overnight at 4°C. The cells were then incubated with secondary antibody, diluted 1:2,000 in 50% IFB (antimouse Alexa-Fluor 488; Molecular Probes) for 1 hr at RT. After six washes with PBS, coverslips were mounted cell side down on glass slides with mounting medium (prolong antifade gold with DAPI [4′,6′-diamidino-2-phenylindole]; Molecular Probes). After images were acquired using confocal microscopy, the existence of perinuclear accumulation in a cell in each image was examined by human eyes.

Nuclear isolation and viral genome quantification

Nuclei were isolated from cell fractionations as previously described,[31] with minor modifications allowing for viral infection. After incubation with rAAV and drugs, cells were washed three times with ice-cold PBS and harvested by centrifugation at 500 g for 10 min. The cell pellet was divided into two aliquots: one for direct viral genome extraction and the other for nuclei isolation. One aliquot was resuspended in hypotonic buffer and homogenized on ice using a Kontes homogenizer to the point where $\sim$90% of cells were broken with nuclei remaining intact. The homogenate was spun at 500 g for 10 min to separate the nuclei from the cytoplasmic components. The purity of nuclear fraction was assured by phase-contrast microscopy and immunoblotting using antitubulin and antilamin A/C antibodies,[33] and no cytoplasmic protein tubulin was detected in purified nucleus (data not shown).

rAAV genomes were recovered from both whole cells and nuclear fraction using DNeasy Blood and Tissue Kit (Qiagen Inc.) according to the manufacturer's protocol. The copy number of rAAV genomes was determined by qPCR on a Light-Cycler 480 using SYBR Green (Roche) as described for viral titering.[31]

Animal studies

Housing and handling of the BALB/c mice and SCID mice used in the current study were carried out in compliance with National Institutes of Health guidelines and approved by the IACUC at the University of North Carolina–Chapel Hill. To grow xenografted breast cancer tumors, 10^6–10^7 MDA-231 breast cancer cells were injected into the mammary fat pad of SCID mice. When the tumor size was about 0.5 cm in diameter, the mice were used for intratumoral injection. Recombinant AAV2 vectors packaging *luciferase* or *GFP* transgenes were administered through the intravenous route (2×10^{10} vgs into tail vein) in a volume of 200 μl PBS or the intratumoral route (1×10^{10} vgs). DMSO or nocodazole (2 mg/kg) were administered via intraperitoneal or intratumoral injection at about 10–12 hr after viral injection. Bioluminescence from luciferase expression was visualized by using a Xenogen IVIS100 imaging system (Caliper Lifesciences) after intraperitoneal injection of luciferin substrate (120 mg/kg of body weight; Nanolight). Image acquisition and analysis were carried out using Living Image software. Quantitative data are based on values from 3 to 4 mice per group.

For vector infusions into mouse brain, animals were anesthetized with isoflurane and placed into a stereotaxic frame. Using a 32-gauge stainless steel injector and a Fisher Scientific infusion pump, mice received 1 μl per hemisphere (total of 5×10^8 vgs) into the striatum over 15 min. The injector was left in place for 3 min after infusion to allow diffusion from the site of injection.

To image viral trafficking in mouse tissues, Cy5-rAAV2 was administrated through intrabrain, intrahepatic, or intratumoral routes. DMSO or nocodazole were administrated through the intraperitoneal route at about 12 hr after viral inoculation. At 1 or 12 hr after vector injection or 4–6 hr after nocodazole injection (16–18 hr after viral injection), animals received an overdose of pentobarbital (100 mg/kg intraperitoneally) and were perfused transcardially with ice-cold 100 m*M* sodium PBS (pH 7.4), followed by 4% PFA in phosphate buffer (PB) (pH 7.4). After tissues were postfixed for 24 hr at 4°C in PFA,[34] 10–20 μm coronal sections were cut using a cyrosection microtome and then the slides were directly sealed with mounting medium (Prolong Antifade Gold with DAPI [4′,6′- diamidino-2-phenylindole]; Molecular Probes).

Quantitative 3D microscopy

Hela cells pulse infected with Cy5-rAAV2 were fixed with PFA and mounted to glass slides as described above. The distribution of viral particles in Hela cells was examined using a Zeiss LSM710 laser scanning confocal microscope equipped with a Plan-Apochromat 63×/NA 1.40 oil objective. Stacks of 20–30 focal planes were captured at 0.31 μm z-intervals through the depth of the cell. 3D images of the cells were reconstructed using the Z-stacks. All images were acquired at pixel dimensions of 0.13 μm × 0.13 μm × 0.31 μm (X, Y, Z) to fulfill the Nyquist sampling.

Deconvolution was performed by the Auto-Deblur software (Media Cybernetics Inc.) using iterative and constrained algorithms as described previously.[32] The procedure started with a theoretical PSF derived from the actual settings of Zeiss710 confocal microscope, including NA of the microscope objective, refractive index of the medium, excitation wavelength, emission wavelength, confocal pinhole radius, pixel size, z-axis interval, and microscope type (i.e., wide field, confocal). A new adjusted adaptive PSF derived from the previous deconvolution round was used to generate the next adaptive PSF that fit the real imaging data better than the previous one (termed as one iteration or deconvolution round). Twelve rounds of iteration were used to deconvolve all the confocal images in this study.

All deconvolved image stacks were processed using the IMARIS software package (Bitplane AG, Zurich, Switzerland) for visualization and quantification as described previously.[32] Briefly, each deconvolved image stack was reconstructed using a volume-rendering module and smoothed by a 3D-median filter. Subsequently, an isosurface-rendering module was applied through thresholding by the fluorescence intensity that was slightly higher than background. For Cy5-rAAV2, the isosurface rendering was thresholded at the fluorescence intensity of 2000 a.u. (the upper boundary of background). For DAPI, isosurface rendering was thresholded at the fluorescence intensity of 3200 a.u.. Parameters (volume, MFI, TFI) for these isosurface-coated Cy5-rAAV2 objects were extracted from the IMARIS program and analyzed to determine the localization of particles as described previously.[32]

Negative staining and electron microscopy

Purified and dialyzed virus particles in 1× PBS were pipetted onto a glow-discharged copper grid. The grid was washed twice with water and then stained with 2% uranyl acetate. Electron microscopy images were taken with a LEO EM 910 transmission electron microscope at various magnifications.

Transient transfection of reporter plasmid and siRNA

For transfection of Hela cells with reporter plasmids, Hela cells were plated at a density of 4×10^5 cells/well and 24 hr later were transfected with TR-CMV-EGFP reporter plasmids using PEI. For each well, 500 ng DNA was mixed with 5 μl PEI (1 mg/ml) in 100 μl of serum-free DMEM and incubated at RT for 10 min before addition to cell medium. Culture medium was refreshed at 6 hr after transfection. At 16–20 hr after transfection, cells were treated with DMSO or other drugs as indicated. At about 20 hr after drug treatments, cells were harvested for flow cytometry analysis of GFP expression as indicated above. The control is the data without any treatment after transfection. The effect of treatments on transgene expression was calculated as 1× data of treatment/positive control.

Knockdown of RhoA was obtained by double transfection of siRNA (Dharmacom, Thermo Scientific) using Nucleofector (Lonza Inc.) performed with an Amaxa Electroporator according to the manufacturer's protocol. Knockdown efficiency was verified by Western blot using RhoA antibody (Abcam Inc.). Efficient knockdown was achieved two days after the first siRNA transfection. After verifying knockdown, approximately two days posttransfection, cells were processed with pulse infection and drug treatments as described above. Viral transduction was analyzed using flow cytometry.

Statistical analysis

Experiments were performed in triplicates and repeated at least three times independently, unless otherwise noted. For studies comparing quantification of luciferase or GFP expression in one treatment group to the corresponding control group, the Student t-test of the mean expression value was performed. For studies comparing quantification of luciferase or GFP expression in more than two treatment groups to the same control group, the one-way analysis of variance (ANOVA) was performed to test the global hypothesis that all mean values are the same across groups. If the global hypothesis is rejected, Dunnett's test was used to compare the mean of each treatment to the mean of control group simultaneously. Luciferase or GFP expression was presented as mean ± SD, and all tests were considered significant if $p < 0.01$, which was indicated by *.

RESULTS

AAV retention in MOTC

AAV is a nonenveloped single-stranded virus and has successfully been used as gene delivery vehicle in clinical trials. To elucidate the role of MTOC in rAAV transduction, we first investigated the intracellular trafficking of rAAV2 over time using viral particles labeled with Cy5. With our optimized protocol, we were able to visualize a single viral particle, and the labeled virions remained as infectious as unlabeled particles.[32] Specifically, homogeneous labeling of virions was achieved by confocal microscopy of labeled particles on glass coverslips (Supplementary Fig. S1A, left; Supplementary Data are available online at www.liebertpub.com/hum). The intensity profile of fluorescent spot followed a single Gaussian distribution, suggesting that the fluorescence signal was from a single particle (Supplementary Fig. S1A, right).[35] The signal had a diameter of about 0.4 μm as determined by Full Width at Half Maximum (FWHM), consistent with the fluorescent signal from other nano-sized viruses.[35] Data from negative staining and electron microscopy demonstrated that the virion structure remained unchanged and that most of the labeled virions were single particles (Supplementary Fig. S1B). To test whether labeling would affect the functionality of the virions, we compared labeled and unlabeled AAV particles in their ability to transduce cells using GFP reporter gene assay. We found that the labeled virions can express GFP transgene as efficiently as the unlabeled ones, indicating that the particles labeled with Cy5 were fully competent at transduction (Supplementary Fig. S1C). It has been relatively difficult to visualize virions on the cell surface presumably because most virions were bound as single particle and the visualization method was not sensitive enough to detect them at single particle level.[33] In contrast, we were able to visualize the AAV particles on the cell surface after 40 minutes of incubation of cells with Cy5-rAAV at 4°C (Supplementary Fig. S1D, left). In addition, the Cy5 fluorescent signal was successfully co-stained with the signal from monoclonal A20 antibody that specifically recognizes the intact rAAV2 capsids (Supplementary Fig. S1D, right). These data demonstrate that our labeling and imaging systems are sufficiently robust and reliable to study the viral trafficking and infection at the level of a single particle.

To study the intracellular trafficking of rAAV, we synchronized particle trafficking using "pulse infection," in which cells are incubated with virions at 4°C for 40 min and unbound virions are then washed away before cells are transferred to 37°C for subsequent viral infection. After pulse infection, we studied the distribution of rAAV particles at several time points over 12 hr (Fig. 1A). During the first 2–4 hr p.i., the majority of viral particles

were scattered in the cytoplasm and trafficking toward the perinuclear region. At 4 hr p.i., the majority of viral particles had finished their cytoplasmic trafficking and localized at the perinuclear region in approximately 30–40% of cells. At 8 hr p.i., perinuclear accumulation was observed in over 80% of cells and persisted for over 6 hr, suggesting retention of viral particles at this perinuclear site (arrows in Fig. 1A). To specifically investigate the role of the perinuclear retention, we focused on the time period between 6 and 8 hr after pulse infection, a time point at which, in majority of cells, most virions have finished cytoplasmic trafficking and remain at the perinuclear region.

Previous studies have co-localized perinuclear rAAV particles to the Golgi apparatus,[36,37] and others have suggested that these virions may co-localize with MTOC.[38] As the perinuclear region is highly crowded and the resolution of classical fluorescent microscopy is only about 0.3 μm in lateral, images solely generated by such fluorescent microscopy alone could falsely co-localize viral particles with many cellular organelles at perinuclear region, namely, Golgi, MTOC, and ER.[38] To effectively discern which cellular structures at the perinuclear region co-localize with AAV particles and retain these virions, we used fluorescence

microscopy and pharmacological interventions (Fig. 1B) to circumvent the above resolution limit issues. Specifically, if rAAV particles do co-localize to and are retained by a particular structure at the perinuclear region, we shall be able to predict that (1) the viral accumulation will be ablated upon the disruption of that structure by pharmacological agents, and (2) the majority of virions will still co-localize with that structure after release from the perinuclear region upon disruption of MTs and MTOC.

Using several antibodies, we demonstrated that rAAV particles can be co-stained with markers for Golgi apparatus and MT-MTOC (peri-MTOC MTs) at the perinuclear region (Fig. 1C). To distinguish whether virus localized to the Golgi or MT-MTOC, we used a panel of pharmacological reagents to disrupt these structures individually and visualized the localization of viral particles in each case. Upon Brefeldin-A treatment to specifically disrupt Golgi apparatus, perinuclear accumulation of AAV was not dispersed (Fig. 1D). In contrast, when MT-MTOC was fully disrupted by nocodazole, the perinuclear localization of AAV was ablated and few rAAV particles co-localized with dispersed Golgi cisternae (Fig. 1E). Although nocodazole treatment affects the Golgi apparatus as well,
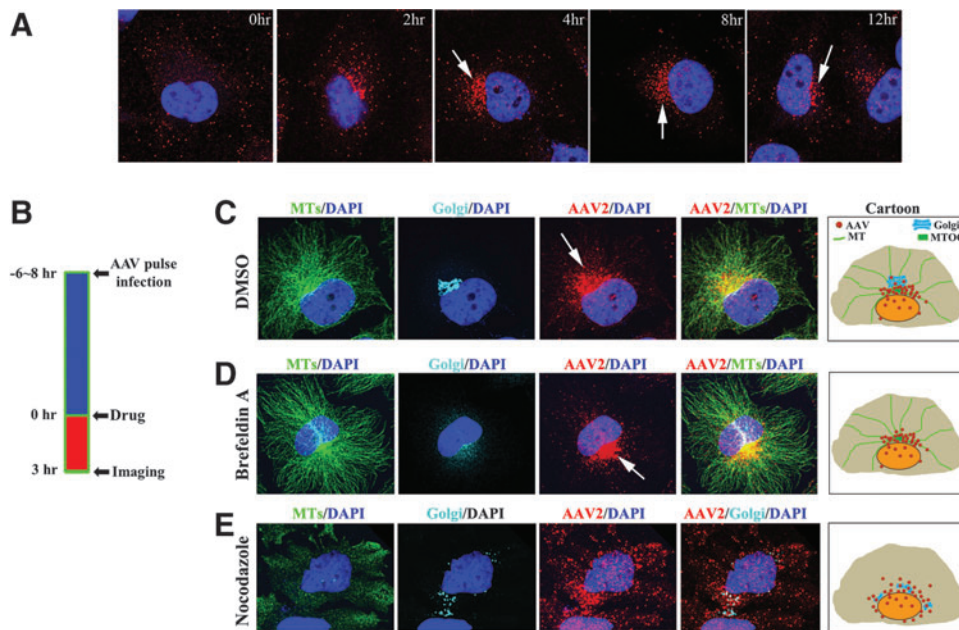

Figure 1. Perinuclear retention of rAAV by MT-MTOC. Hela cells were fixed to examine the distribution of Cy5-labeled viral particles at various time points after pulse infection. Nuclei were stained with DAPI (blue). **(A)** Representative images showing the distribution of intracellular rAAV2 over 12 hr after viral inoculation. Arrows indicate perinuclear accumulation in the cells. **(B)** Schematic diagram showing the procedure used for drug intervention and confocal imaging experiments. **(C–E)** Confocal images showing the localization of MT-MTOC, Golgi apparatus, and rAAV2 when cells were treated with DMSO **(C)**, 2 μg/ml Brefeldin-A **(D)**, and 30 μM nocodazole **(E)**. MTs were stained with α-tubulin antibody (green) and Golgi apparatus was stained with Giatin antibody (cyan). Arrows indicate the perinuclear accumulation of rAAV. The right most panels in **(C–E)** display schematic cartoons showing the localization of rAAV particles, Golgi, and MTs in the cells. DAPI, 4′,6-diamidino-2-phenylindole; rAAV, recombinant adeno-associated virus; MT-MTOC, microtubules at microtubule-organization center.

based on the result from treatment of Brefeldin A and nocodazole, these data suggest that rAAV is co-localized to and retained by MT-MTOC but not Golgi apparatus at the perinuclear region. This finding is consistent with previous studies that show that many other viruses traffic and localize to MTOC or MT-MTOC.[10,14,39,40]

Disruption of MT-MTOC retention increases AAV transduction

To study whether the retention of AAV in MTOC affects rAAV transduction, we also used anti-MT drugs (nocodazol, colchicine, rhizoxin, and maytansine) to disrupt MTs as described in Fig. 2A. We infected 293 cells with AAV vector encoding *GFP* transgene. Eight hours later, drugs were added to the cells for 4 hr and washed out. The cells with GFP expression were analyzed by flow cytometry at 20 hr after nocodazole treatment (Fig. 2A). To exclude potential effects of the reagents on the second strand synthesis of viral DNA, self-complementary rAAV (rAAV2-CMV-GFPsc) was used in the transduction assay.

Disruption of MTs by nocodazole treatment induced a 2–4-fold increase in viral transduction in multiple cell lines as measured by the expression of the transgene *GFP* (Fig. 2B). To rule out the possibility that the increased viral transduction was specific to nocodazole, a panel of anti-MT drugs (AMDs) was used (colchicine, rhizoxin, maytansine), all of which disrupt MTs. Similar increases in GFP expression were observed with all of the drugs (Fig. 2C). We also tested whether stabilization of MT-MTOC by taxol would reverse the effect of nocodazole, by comparing the viral transduction in cells treated with nocodazole alone or with nocoda-

zole and taxol. We found that co-administration of taxol with nocodazole restored the enhanced viral transduction to the control level (Fig. 2D). Together, these results demonstrated that MT-MTOC disruption is able to increase rAAV transduction.

Increased transduction upon MT-MTOC disruption is independent of promoter activity, cell cycle arrest, and viral degradation

Next, we explored the underlying mechanism associated with the increase in viral transduction induced by MT-MTOC disruption. We envisioned three possible mechanisms for the increase in transgene expression: (1) MT-MTOC disruption leads to the activation of the promoter on the viral transgene cassette; (2) MT-MTOC disruption results in cell cycle arrest that, in turn, leads to increased viral transduction; (3) MT-MTOC disruption affects intracellular viral processing or trafficking. First, we employed *in vitro* plasmid transfection to examine the potential effect of MT-MTOC disruption on promoter activity. Our flow cytometry data demonstrated that MT-MTOC disruption by AMDs did not affect the reporter gene (GFP) expression from the viral transgene cassette, which was directly transfected into the cells using PEI (Fig. 3A). This excludes the possibility of AMD treatment affecting promoter activity (mechanism 1). To test the second possible mechanism, we measured the effects of AMD treatment on viral transduction in cells whose cell cycle was already arrested at S-phase by double thymidine block, a step preceding the M-phase block caused by AMDs. Our data showed that MT-MTOC disruption also induced an enhancement of viral transduction in these prearrested cells, suggesting
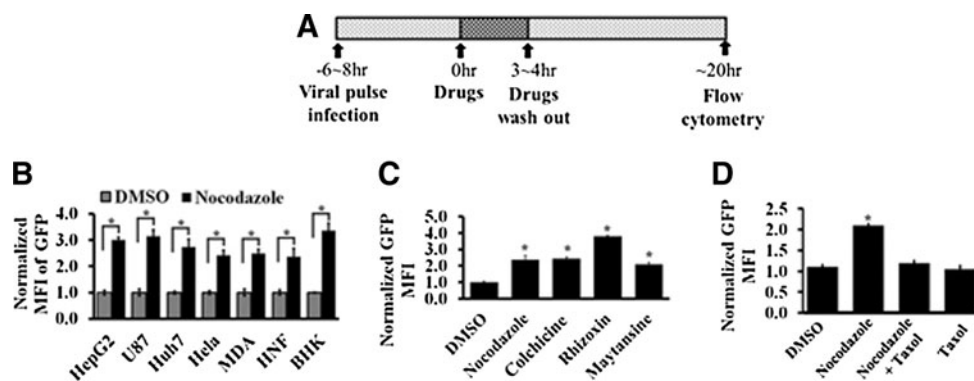

Figure 2. Disruption of MT-MTOC increases rAAV transduction. **(A)** Schematic diagram showing the procedure used for the experiments. **(B)** A variety of cell lines used to measure rAAV2 transduction with and without nocodazole treatment. MFI of GFP expression is normalized to the DMSO treatments. **(C)** rAAV2 transduction was determined by MFI of GFP expression in Hela cells treated with various AMDs. **(D)** The MFI of GFP expression was measured in cells treated with DMSO, nocodazole, nocodazole+taxol, or taxol only. *Statistically significant difference with $p < 0.01$. AMDs, anti-MT drugs; MFI, mean fluorescence intensity.
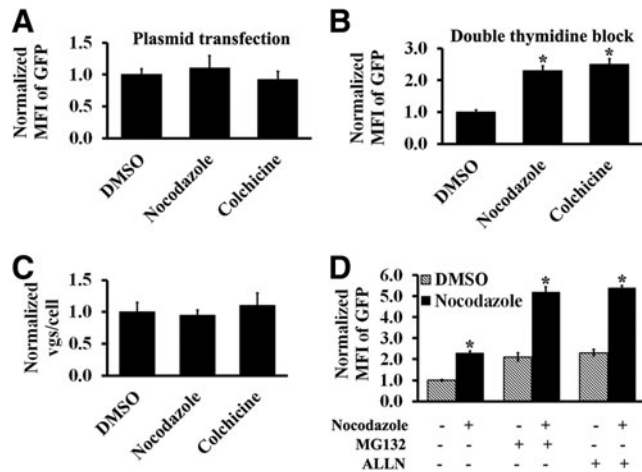
Figure 3. MT-MTOC disruption does not affect promoter activity and viral degradation. **(A)** At 16–20 hr after transfection with plasmid TR-CMV-GFP using polyethyleneimine (PEI), Hela cells were treated with drugs for 3 hr. At approximately 20 hr after drug treatments, cells were harvested for flow cytometry analysis to measure the GFP expression. **(B)** Cell cycle of cells was arrested using a double-thymidine block and MT-MTOC was disrupted as in Fig. 2A and rAAV transduction was then measured. **(C)** Cells were treated as in Fig. 1B, and quantitative PCR (qPCR) was used to determine the copy number of the viral genome. **(D)** Cells were treated as in Fig. 2A except that proteasome inhibitors were added with AMD at the same time after infection and transduction was measured. *Statistically significant difference between DMSO and nocodazole treatments with $p < 0.01$. AMD, anti-MT drugs.

that the increase in viral transduction was independent of cell cycle arrest induced by disruption of MT-MTOC (mechanism 2; Fig. 3B). Additionally, it was previously reported that intracellular degradation of rAAV limits viral transduction and its blockage using proteasome inhibitors resulted in dramatic increase in viral transduction.[41] It was also previously proposed that MT-MTOC facilitates the degradation of intracellular proteins by transporting these proteins to and retaining proteasome machineries at the perinuclear region. As a result, we tested if MT-MTOC disruption has reduced the rAAV degradation. Data from quantitative PCR demonstrate that the amount of rAAV measured as genome copy number (vgs/cell) was not significantly changed upon MT-MTOC disruption, suggesting that AMD treatment did not affect the viral degradation (Fig. 3C). This notion was further supported by our data from pharmacological intervention studies that showed that proteasome inhibitor can further enhance viral transduction if co-administrated with AMDs (Fig. 3D). Therefore, we have excluded the hypotheses (1) that MT-MTOC disruption directly increases transgene expression, (2) that MT-MTOC disruption acts to increase transduction through cell cycle arrest, and (3) that MT-MTOC disruption in-

creases rAAV transduction by decreasing the degradation of rAAV virions.

Interestingly, previous studies, including ours, demonstrated that disruption of MTs during rAAV entry has a negative effect on transduction because of impaired cytoplasmic trafficking.[30] The data from previous study and our current findings suggest that (1) MTs are not required for later steps of transduction after rAAV trafficking to perinuclear region because MT disruption did not inhibit rAAV transduction after that time, and (2) though MTs play a central role in trafficking of the virus to the perinuclear region, at later time points these structures act to retain virions and thus limit transduction. It is unclear how rAAV accumulates at MTOC and whether any motors are involved in the process; further studies are warranted.

Nuclear entry of rAAV is increased upon the disruption of MT-MTOC

Based on the above findings, the most likely mechanism for elevated viral transduction upon MT-MTOC disruption occurs at the level of trafficking. It has been previously demonstrated that nuclear entry is an essential trafficking event for rAAV's infectious pathway.[42,43] Moreover, nuclear entry is the most probable event subsequent to and being limited by perinuclear retention in rAAV's infectious trafficking pathway. We hypothesized that the retention of viral particles at the MTOC region may limit the subsequent nuclear trafficking of the virus. To test this hypothesis, we visualized viral trafficking steps with and without Nocodozole treatment by fluorescent confocal microscopy and quantitatively evaluated the distribution of viral particles at different time points after administration of nocodazole at 6–8 hr p.i. (Fig. 4A). At about 1–1.5 hr after MT-MTOC disruption (~8–9 hr p.i.), the perinuclear retention of rAAV particles was ablated in most cells examined (Fig. 4C) and the viral particles spread around the outside of nucleus (Fig. 4B). Later, ~3–4 hr after MT-MTOC disruption (~10–11 hr p.i.), an approximate 2-fold increase of viral particles was observed in the nucleus as shown by the representative images from confocal microscopy (Fig. 4B, C) and quantitative data from 3D microscopy (Fig. 4B-f/i/l, and 4D). Increased viral entry into the nucleus was also supported by quantitative PCR analysis of the viral genome copy number in the nuclear fractions of treated and untreated cells (Fig. 4E). Together, these results suggest that disruption of MT-MTOC at 6–8 hr p.i. leads to an increase in the fraction of viruses in nuclear proximity and may explain the increased transduction we have observed (Fig. 2).
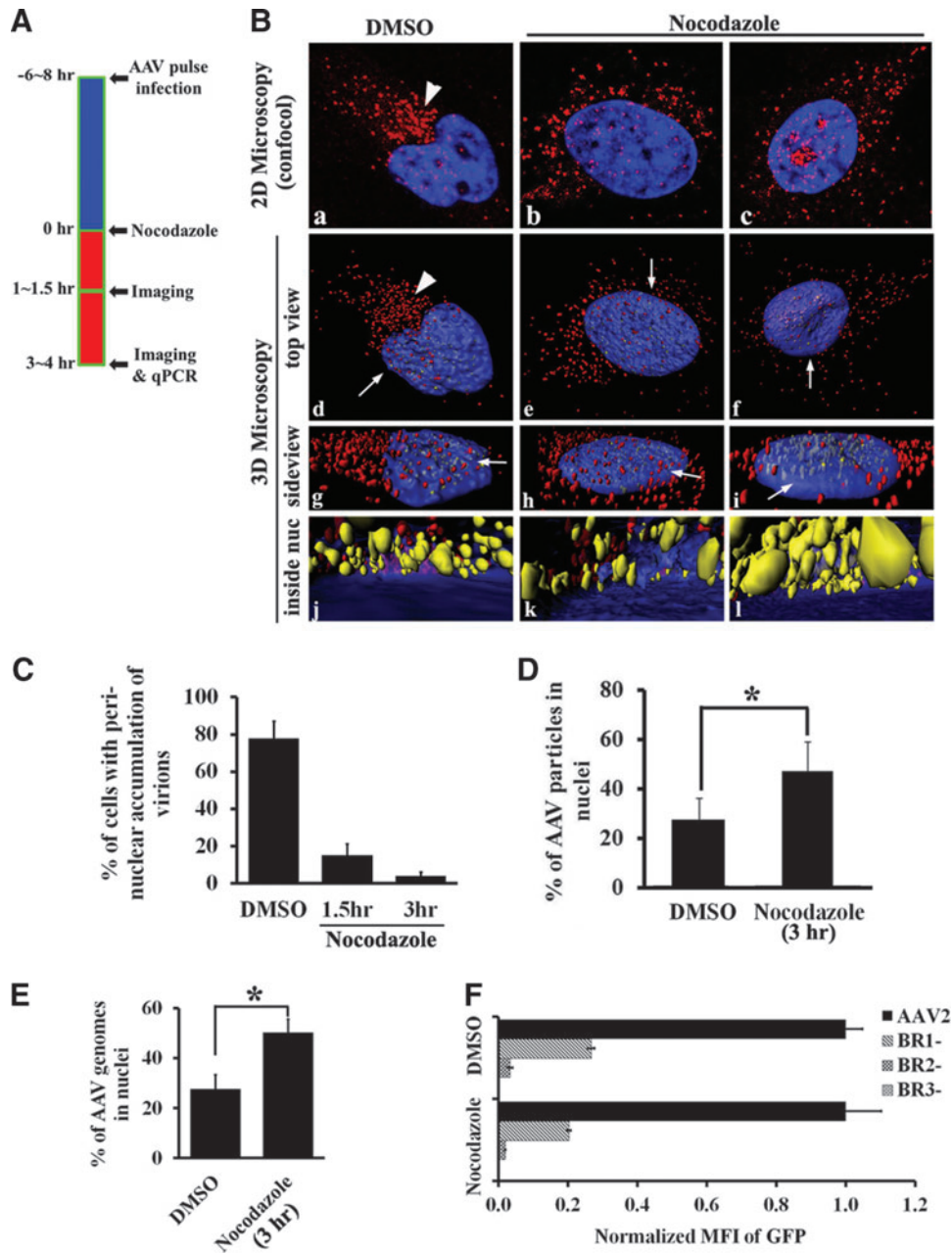
Figure 4. Release of rAAV and increased nuclear entry upon MT-MTOC disruption. **(A)** Schematic diagram showing the procedure for the experiments in **(B–E)**. Specifically, Hela cells were treated with DMSO or nocodazole at 6–8 hr after pulse infection of Cy5-rAAV2 and fixed at 1–1.5 hr or 3–4 hr after drug treatments. Nuclei were stained with DAPI (blue). **(B)** Representative images from 2D confocal microscopy of one focal plane **(a–c)** and 3D images reconstructed from confocal Z-stacks as described in Materials and Methods. **(d–l)** Viral distribution in cells treated with DMSO **(a, d, g, j)** or with nocodazole for 1–1.5 hr **(b, e, h, k)** or 3–4 hr **(c, f, i, l)**. **(d–f)** are top views, whereas **(g–i)** are magnified side views from directions indicated by arrows in **(d–f)**, respectively. **(j–l)** are views observed inside the nucleus (from the directions indicated by arrows in **(g–i)**, respectively, between the top and bottom nuclear envelopes, which is indicated by the blue layer based on the DAPI signal). rAAV2 particles in cytoplasm are highlighted in red and those inside the nucleus highlighted in yellow. **(C)** The proportion of cells with perinuclear accumulation of rAAV particles after DMSO or nocodazole treatment (for 1.5 or 3 hr) was quantified in 50–100 cells for each group. The perinuclear accumulation is defined as concentrated viral particles at a single perinuclear region (arrows in Fig. 2 and arrowheads in Fig. 5B). **(D)** The proportion of rAAV particles entering nucleus in cells treated with DMSO or nocodazole at 3 hr was quantified from the 3D microscopy data (Fig. 5B). From each group, 20–30 cells were used for the 3D quantitative microscopy described in Materials and Methods. **(E)** Nuclei were fractioned from cells and qPCR was used to determine the copy number of rAAV genomes in the nucleus of cells treated with nocodazole for 3 hr, in comparison with DMSO-treated cells. **(F)** Cells were treated with DMSO or nocodazole as described in Fig. 1A and then transduced with AAV or BR mutants of AAV, and transduction was analyzed by flow cytometry. GFP expression is normalized to that in DMSO-treated group. *Statistically significant difference between DMSO and nocodazole treatments with $p < 0.01$.

Three major basic regions (BRs) on the capsid have been shown to function as nuclear localization signals (NLS) with varying strength.[42,43] rAAV mutants with deletions at these regions can still accumulate at the perinuclear region but are unable to enter nucleus.[37] Our prior study has demonstrated that pronounced Golgi localization is observed with the BR1 mutant, and the BR2 and BR3 capsid mutants appear to have diffuse localization throughout the cell in addition to localizing to the Golgi.[37] To test whether NLS are required for the increased nuclear entry and viral transduction, we examined the effects of MT-MTOC disruption on these BR deletion mutants. In both DMSO- and nocodazole -treated cells, BR deletions resulted in the reduced viral transduction (Fig. 4F). Importantly, nocodazole treatment was unable to restore the impaired transduction of these BR mutants, indicating that AMD-induced enhancement of viral transduction and nuclear entry requires the capsid NLSs. These data suggest that MT-MTOC disruption releases rAAV to continue down its normal nuclear entry pathway and does not cause rAAV's nuclear entry pathway to change.

rAAV is imported into the nucleus via the RhoA-ROCK-Actin pathway upon MT-MTOC disruption

The above findings suggested that MT-MTOC disruption itself allows only the release of rAAV particles from the perinuclear region. The subsequent increase in nuclear entry is achieved by a mechanism that requires the NLS on viral capsid. It is well established that MT disruption can lead to RhoA-ROCK mediated rearrangement of actin filaments (AFs), which in turn may affect actin-mediated intracellular trafficking.[44,45] Perinuclear AFs have been suggested to be involved in nuclear import/export of intracellular materials via association with the nuclear envelope or perhaps nuclear pore complexes.[10,46–55] In this study, we tested whether the AFs regulated by the activation of RhoA-ROCK upon MT disruption contributed to the increased rAAV nuclear entry and transduction. First, we transiently transfected siRNA to knockdown the expression of endogenous RhoA as demonstrated by immunoblotting for the RhoA protein (Fig. 5A). Interestingly, treatment with nocodazole induced an increase in viral transduction only in cells transfected with the control (scrambled) siRNA and had minimal effect in RhoA knockdown cells (Fig. 5B). This observation suggests that enhanced AAV transduction via MTOC disruption requires RhoA activation. H1152 is a potent inhibitor of ROCK, a downstream effector of

RhoA, and induces actin filament alterations. Cytochalasin D (CytoD) is an inhibitor of AFs that induces the de-polymerization of these filaments.[56] Both H1152 and CytoD were found to ablate the transduction enhancement induced by MT-MTOC disruption with nocodazole; therefore, the enhancement of transduction required that ROCK not be inhibited and that AFs be intact (Fig. 5C). The data suggest that the RhoA-ROCK-Actin pathway is required for the increased viral transduction upon MT-MTOC disruption. Visualization of viral particles by fluorescence microscopy revealed that nocodazole -induced viral dispersion from the perinuclear region was unaffected by co-administration with H1152 or CytoD (Fig. 5D). Our results from 3D quantitative microscopy further demonstrated that co-administration of either H1152 or CytoD blocked the increase in viral nuclear entry only after MT-MTOC disruption (Fig. 5E). Additionally, administration of H1152 or CytoD alone at 6–8 hr p.i. did not affect the transduction and nuclear entry of rAAV (Fig. 5C, E).

Together, the above data suggest a two-step working mechanism for the increased rAAV transduction observed upon MT-MTOC disruption: (1) viral particles are released from the perinuclear region and spread around the outside of the nucleus upon MT-MTOC disruption, and (2) some of these viral particles are then transported into the nucleus via the RhoA-ROCK-Actin pathway.

Perinuclear retention of rAAV and nocodazole-mediated enhancement on viral transduction also occur *in vivo*

In cell culture, we observed a bottleneck in viral transduction at the stage of accumulation and retention of rAAV at MTOC region. rAAV is currently widely used as a gene therapy vector in many clinical trials to tackle a variety of human diseases.[27] The effort to improve its efficiency in gene delivery has been compromised by the lack of knowledge about rAAV trafficking in *in vivo* settings. With the sensitive imaging technique used in this study, we examined whether perinuclear retention of rAAV also acted as a bottleneck *in vivo*. To examine this hypothesis, we injected Cy5-rAAV into mouse brain, liver, or xenografted tumor, and determined the viral distribution at different time points after viral infection. At an early stage (~1 hr) after viral inoculation, viral particles were scattered across cells in these tissues, as is clearly observed in the brain image (Fig. 6A). Because of the relatively high background fluorescence observed in both liver and xenografted tumor, we were not able to visualize single viral particles in
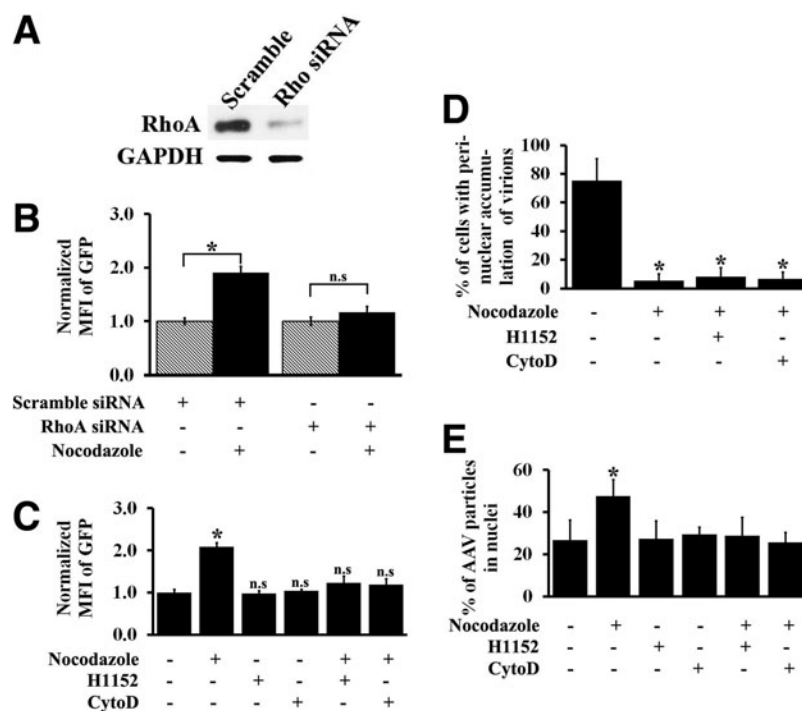
Figure 5. Disruption of MT-MTOC increases viral transduction and nuclear entry through an RhoA-ROCK-Actin pathway. **(A)** Immunoblot showing the siRNA-mediated transient knockdown of the RhoA protein in Hela cells. Scramble siRNA used as a control. **(B)** The level of rAAV transduction was measured in Scramble or RhoA siRNA-transfected cells treated with or without nocodazole treatment at 6–8 hr after rAAV infection. **(C)** The level of rAAV transduction was determined in cells treated with DMSO or nocodazole alone or in combination with H1152 or CytoD. **(D)** The proportion of cells with perinuclear accumulation of rAAV particles was measured in the presence of DMSO or nocodazole alone or in combination with H1152 or CytoD. **(E)** The proportion of rAAV particles in the nucleus was determined in cells treated with DMSO or nocodazole alone or in combination with H1152 or CytoD. *Statistically significant difference between DMSO only and other drug treatments with $p < 0.01$.

these tissues as observed in the brain; instead, we were able to visualize particles only at the sites of viral injection, where a higher concentration of labeled virions was present (arrowheads in Fig. 6A). At 6–12 hr p.i., a large number of viral particles were observed to accumulate at the perinuclear region, consistent with our *in vitro* studies (Fig. 6A). Approximately 60–80% of cells in these tissues had perinuclear accumulation by 12 hr after infection (arrows in Fig. 6A, B).

Furthermore, we tested whether AMD treatment could disrupt this perinuclear retention and increase viral transduction in mouse as was observed in our *in vitro* studies. Approximately 10 hr after viral inoculation, nocodazole was administrated to the animal through intraperitoneal or intratumoral injection. At 4–6 hr after nocodazole injection ($\sim$14–16 hr p.i.), perinuclear retention (arrows in Fig. 7A) was observed only in DMSO-treated animals and was ablated in the cells of both liver and xenografted breast tumor in nocodazole - treated animals (Fig. 7A). Using *GFP* as a reporter gene packaged by rAAV, a significantly stronger GFP fluorescent signal was observed in the nocodazole-

treated breast tumors (Fig. 7B). Moreover, by measuring luciferase activity using the IVIS imaging system, we observed a roughly 10-fold increase of viral transduction in both liver and xenografted tumor of nocodazole-treated mice (Fig. 7C, D). Together, these data suggest that rAAV takes a similar subcellular trafficking route in animal tissues to that *in vitro* and is retained at the perinuclear region, a trafficking bottleneck for viral transduction.

DISCUSSION

Viral accumulation at the perinuclear region is commonly observed during the infection of many viruses (e.g., Ad, HSV, HIV, influenza, parvoviruses).[11,13–15,39] However, it remains unclear regarding whether and how this accumulation affects viral infection. Two plausible hypotheses[9] are (1) viruses exploit the cellular protein-trafficking machineries to approach the replication site or to concentrate viral components for viral replication and later virion assembly, thus supporting viral infection, and (2) perinuclear accumulation represents an innate cellular response that recognizes virus
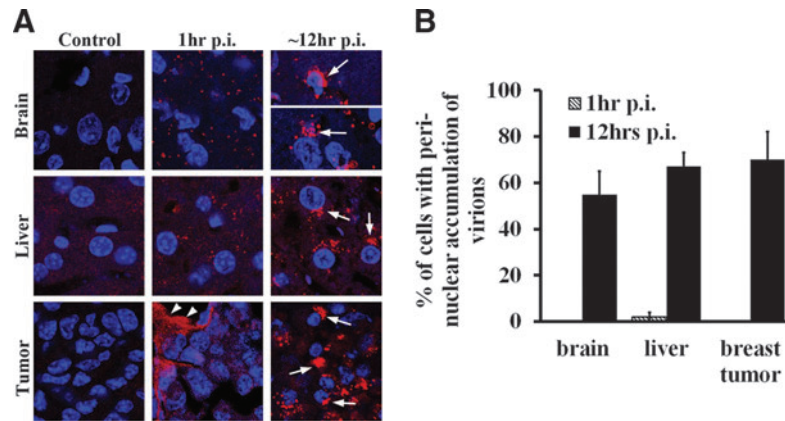
Figure 6. Perinuclear accumulation of rAAV in mouse tissues. Mouse tissues (brain [cerebrum], liver, xenografted breast tumor) were removed at 1 or 12 hr after injection of Cy5-rAAV and sectioned using a cryo-microtome. Nuclei are stained with DAPI (blue). The viral particles were visualized by confocal microscopy. **(A)** Representative confocal images showing the viral distribution in uninfected mouse tissues (control) or tissues that were infected with rAAV for 1 or 12 hr. Arrowheads indicate concentrated rAAV at the injection site. Arrows indicate perinuclear accumulation of virions. **(B)** The percentage of cells with perinuclear accumulation of rAAV in each tissue was measured at 1 hr postinfection (p.i.) and 12 hr p.i. For each group 50–100 cells were analyzed.

components as foreign or misfolded proteins and targets them for sequestration and degradation at the perinuclear region, thus interfering with viral infection. Our present study has supported the hypothesis that perinuclear accumulation is a cellular defense mechanism to sequester virions in order to limit the infection of rAAV.

Both Golgi and MTOC are perinuclear structures that coincidentally co-localize at the perinuclear region with many viruses.[10,11,13–16] However, it
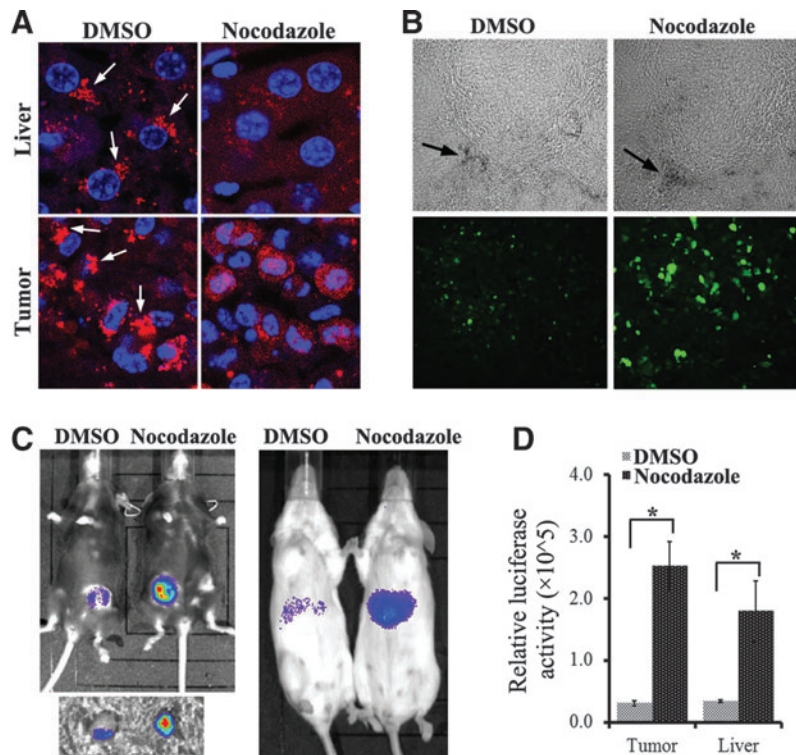

Figure 7. Disruption of perinuclear accumulation of rAAV particles with nocodazole treatment increases transduction *in vivo.* **(A)** Representative images showing the distribution of rAAV particles (red) in tissues treated with DMSO or nocodazole. Nuclei are stained with DAPI (blue). Arrows indicate the perinuclear accumulation of virions. **(B)** Representative images showing the viral injection sites as visualized with injected India ink (arrows on the upper panel) and transgene GFP expression (green in lower panel) in the xenografted tumors. **(C)** IVIS imaging of luciferase signal in xenografted breast tumor and liver at 1 week after viral injection. Left panel shows the luciferase activity in the xenografted tumor before (upper image) or after (lower image) removal from the mice. Right panel shows the luciferase activity from liver expression. **(D)** The relative luciferase activity in the tumor and liver was quantitated as photons/sec/cm^2 ($n = 3$–4). *Statistically significant difference between DMSO and nocodazole treatments with $p < 0.01$.

remained unclear which cellular structure maintains perinuclear accumulation of rAAV. Earlier studies have suggested that the perinuclear viral particles co-localize to the Golgi apparatus.[36,37] Another study suggests that these virions may co-localize with MTOC.[38] In this study, to examine which structure was involved, we used confocal fluorescence microscopy and pharmacological intervention to circumvent the difficulties in studying the interactions between virions and cellular structures at the highly crowded perinuclear region because of the resolution limits of classical fluorescence microscopy ($\sim 0.3\,\mu m$ in lateral). Our results suggest that MT-MTOC but not the Golgi co-localizes with and retains the rAAV particles at perinuclear region (Fig. 1). Consistent with our findings, many other viruses, including Ad, HSV, and HIV, have also been shown to move on MTs to the MTOC region and associated with MT-MTOC.[10,14,39,40,57–62] Furthermore, Fig. 1E shows that only a small portion of viral particles co-localized with the dispersed Golgi cisternae, which are released from highly packed MTOC region upon MT-MTOC disruption. This suggests that fewer particles physically localize in the Golgi apparatus. Consistent with previous reports, we did find that disruption of the Golgi apparatus at an earlier time during infection could impair rAAV transduction (data not shown). These data indicate that the Golgi does play a role in viral infection, probably through modification of viral capsid critical for viral infection, but is dispensable for perinuclear retention of incoming virions. Further investigation of the exact role of the Golgi apparatus on the infection of rAAV may advance our current knowledge of virology.

Our results, together with previous studies, strongly suggest that perinuclear retention by MTOC during early infection serves as a cellular barrier limiting viral transportation to the replication sites and leads to decreased viral transduction. During early infection stage, in which a virus delivers its genome to the target site for replication, accumulation of incoming virions at MTOC region is observed for most viruses that exploit MTs for earlier cytoplasmic trafficking.[10–15,39] Consistent to these findings, we demonstrated that retention of rAAV by MT-MTOC limits viral transduction, and that disruption of MT-MTOC during infection led to an increase in rAAV transduction (Fig. 2E). Strikingly, some viruses may have evolved to overcome the MTOC retention by breaking MTs during their infection.[18–22] For instance, HSV dismantle MT-MTOC after entering the cells as one of the functions of viral protein ICP0 and deletion of ICP0 seems to limit viral infection.[21]

Our current study raises an interesting question for future exploration, which is whether and how the endosomal vesicles at MTOC region may contribute to the rAAV transduction enhancement observed upon MT-MTOC disruption. A reasonable hypothesis is that at 6–8 hr p.i., some viral particles observed at the MTOC region still remain inside the MT-localized endosomes/lysosomes,[32,63] whereas others have escaped the endosomes and directly associated with MTs. Direct interaction between MTs and the rAAV capsid has been demonstrated previously.[64] Both endosomal and escaped viral particles would be released from the MTOC region upon MT-MTOC disruption. Using rAAV mutants with defects in the phospholipase (PLA) domain that helps rAAV for endosome escape,[37] we determined that MT-MTOC disruption was unable to rescue the impaired viral transduction of these mutants (data not shown), which suggests that MT-MTOC disruption does not promote the escape of rAAV from endosomes. Further experiments should be performed to test whether nocodazole-mediated RhoA activation is not involved in endosome escape in the MTOC region with PLA mutant. Furthermore, increased viral particles reaching the nucleus upon disruption of MT-MTOC are most likely the subset of virions that have escaped from endosomes and are directly associated with MTs. Those virions that failed to escape endosomes are not eligible for nuclear entry regardless of the integrity of MT-MTOC. This notion is consistent with our observation that the proportion of nuclear particles increases from only about 30% to 50%, possibly because about 30–40% of virions are still inside the endo/lysosomes at 8 hr p.i.[32] In the future, it will be interesting to investigate the potential role of endo/lysosomal vesicles on viral retention at the perinuclear region, which would add valuable information to the mechanism of this perinuclear phenomenon. Additionally, the relationship of free rAAV particles in the cytoplasma with MT should be elucidated.

Actin filaments (AFs) and small Rho GTPases have been shown to be involved in viral infection, including cell entry, cytoplasmic trafficking, and nuclear entry.[36,56,65–67] Recently, perinuclear and nuclear AFs were shown to associate with the nuclear envelope and nuclear pore complex, and were suggested to be involved in nuclear transport of macromolecules and viral particles.[46–50,66] rAAV has been suggested to utilize AFs to enter nucleus during an earlier stage of infection when MTs were disrupted.[30] Furthermore, the disruption of MTs leads to a RhoA-ROCK-mediated rearrangement of AFs.[44,45] Consistent with these studies, our data

show that AFs may facilitate the increase in nuclear entry through the RhoA-ROCK pathway upon MT-MTOC disruption (Fig. 5). Interruption of this pathway in the presence of intact MTs does not affect the level of viral transduction. This finding indicates that, at this time point, nuclear import of rAAV by AFs occurs only upon the disruption of MT-MTOC. It is possible that the AAV capsid has a much higher binding affinity for MTs than for AFs, and therefore remains associated with MT-MTOC. Moreover, the requirement of RhoA and ROCK activity indicates that MT disruption-induced alterations of AFs are necessary for the increase in viral nuclear entry and transduction. One possibility is that activated RhoA-ROCK results in more AFs connecting to the nuclear pore complex, which in turn transports more rAAV particles into the nucleus. Further study of this mechanism will add more detail to current knowledge of viral nuclear entry as well as the biology of cellular cytoskeletons.

Although tremendous progress has been made in understanding the trafficking of rAAV virions in cell culture, little is known about the trafficking pattern of this virus *in vivo*. This has limited one's ability to improve the efficiency of viral transduction for gene delivery in its natural environment. In this study, we examined the trafficking of rAAV in mouse tissues, including brain, liver, and xenografted tumors. In each of these tissues, the viral particles accumulate at a perinuclear site, resembling our *in vitro* observations (Fig. 6). Treatment with nocodazole was able to disrupt the perinuclear retention of rAAV and increase the viral transduction in all tissues tested (Fig. 7). Although further investigations are needed to refine the details of viral trafficking in these tissues, to our best knowledge, this is the first study to verify an *in vitro* trafficking pathway in *in vivo* settings. Additionally, the data showing that nocodazole treatment can enhance rAAV transduction in breast cancer cells indicate that there may be a synergistic effect between chemotherapeutic drugs, such as AMDs, and rAAV-mediated gene therapy in treating cancer patients. In this study, we studied the enhancement effect of MT-MTOC disruption after virus entry on rAAV2 transduc-

tion. Since different serotypes of AAV may use different mechanism for intracellular trafficking, it should be warranted whether the MT disruption also has an enhanced effect on transduction from other serotypes of AAV after cell entry.

In summary, our current study examined the mechanism of perinuclear retention of the parvovirus AAV and the corresponding effects on viral infection. Our data demonstrated that perinuclear retention by MT-MTOC serves as a subcellular barrier and limits rAAV infection, specifically at the step of nuclear entry, providing a novel host defense mechanism to sequester incoming virions. These studies may shed light on mechanisms of viral pathogenesis, especially under circumstances of MT disassembly during cell division and that of MTOC malfunction caused by misfolded-protein diseases or treatment with chemotherapy drugs. Moreover, further understanding of the determinants on the virus responsible for perinuclear retention may also lead to novel strategies for the enhancement of rAAV vector for gene delivery.

AUTHOR DISCLOSURE

R.J.S. is the founder and a shareholder at Asklepios BioPharmaceutical. He receives research support through the University of North Carolina (UNC) from Asklepios BioPharmaceutical. He holds patents that have been licensed by UNC to Asklepios Biopharmaceutical, for which he receives royalties. He has consulted for Baxter Healthcare and has received payment for speaking.

REFERENCES

1. Bruce Alberts AJ, Lewis J, Raff M, et al. Molecular Biology of the Cell. 4th edition. (Garland Science, New York, NY); 2002. Cell Biology of Infection. Available from: www.ncbi.nlm.nih.gov/books/NBK26833/

2. Brinkley BR. Microtubule organizing centers. Ann Rev Cell Biol 1985;1:145–172.

3. Giannakakou P, Sackett DL, Ward Y, et al. p53 is associated with cellular microtubules and is transported to the nucleus by dynein. Nat Cell Biol 2, 709–717.

4. Niklinski J, Claassen G, Meyers C, et al. Disruption of Myc-tubulin interaction by hyperphosphorylation of c-Myc during mitosis or by constitutive hyperphosphorylation of mutant c-Myc in Burkitt's lymphoma. Mol Cell Biol 2000;20:5276–5284.

5. Ziegelbauer J, Shan B, Yager D, et al. Transcription factor MIZ-1 is regulated via microtubule association. Mol Cell 2001;8:339–349.

6. Roth DM, Moseley GW, Glover D, et al. A microtubule-facilitated nuclear import pathway for cancer regulatory proteins. Traffic 2007;8:673–686.

7. Gong K, Xing D, Li P, et al. cGMP inhibits TGF-beta signaling by sequestering Smad3 with cytosolic beta2-tubulin in pulmonary artery smooth muscle cells. Mol Endocrinol 2011;25:1794–1803.

8. Garcia-Mata R, Gao YS, Sztul E. Hassles with taking out the garbage: Aggravating aggresomes. Traffic 2002;3:388–396.

9. Wileman T. Aggresomes and pericentriolar sites of virus assembly: Cellular defense or viral design? Annu Rev Microbiol 2007;61:149–167.

10. Sodeik B, Ebersold MW, Helenius A. Microtubule-mediated transport of incoming herpes simplex virus 1 capsids to the nucleus. J Cell Biol 1997;136:1007–1021.

11. Dohner K, Wolfstein A, Prank U, et al. Function of dynein and dynactin in herpes simplex virus capsid transport. Mol Biol Cell 2002;13:2795–2809.

12. Suikkanen S, Saajarvi K, Hirsimaki J, et al. Role of recycling endosomes and lysosomes in dynein-dependent entry of canine parvovirus. J Virol 2002;76:4401–4411.

13. Mani B, Baltzer C, Valle N, et al. Low pH-dependent endosomal processing of the incoming parvovirus minute virus of mice virion leads to externalization of the VP1 N-terminal sequence (N-VP1), N-VP2 cleavage, and uncoating of the full-length genome. J Virol 2006;80:1015–1024.

14. Yea C, Dembowy J, Pacione L, et al. Microtubule-mediated and microtubule-independent transport of adenovirus type 5 in HEK293 cells. J Virol 2007;81:6899–6908.

15. Boisvert M, Fernandes S, Tijssen P. Multiple pathways involved in porcine parvovirus cellular entry and trafficking toward the nucleus. J Virol 2010;84:7782–7792.

16. Liu SL, Zhang ZL, Tian ZQ, et al. Effectively and efficiently dissecting the infection of influenza virus by quantum-dot-based single-particle tracking. ACS Nano 2012;6:141–150.

17. Bukrinskaya A, Brichacek B, Mann A, et al. Establishment of a functional human immunodeficiency virus type 1 (HIV-1) reverse transcription complex involves the cytoskeleton. J Exp Med 1998;188:2113–2125.

18. Avitabile E, Di Gaeta S, Torrisi MR, et al. Redistribution of microtubules and Golgi apparatus in herpes simplex virus-infected cells and their role in viral exocytosis. J Virol 1995;69:7472–7482.

19. Ploubidou A, Moreau V, Ashman K, et al. Vaccinia virus infection disrupts microtubule organization and centrosome function. EMBO J 2000;19:3932–3944.

20. Schepis A, Schramm B, de Haan CA, et al. Vaccinia virus-induced microtubule-dependent cellular rearrangements. Traffic 2006;7:308–323.

21. Liu M, Schmidt EE, Halford WP. ICP0 dismantles microtubule networks in herpes simplex virus-infected cells. PLoS One 2010;5:e10975.

22. Martin D, Duarte M, Lepault J, et al. Sequestration of free tubulin molecules by the viral protein NSP2 induces microtubule depolymerization during rotavirus infection. J Virol 2010;84:2522–2532.

23. Sfakianos JN, Hunter E. M-PMV capsid transport is mediated by Env/Gag interactions at the pericentriolar recycling endosome. Traffic 2003;4:671–680.

24. Nozawa N, Yamauchi Y, Ohtsuka K, et al. Formation of aggresome-like structures in herpes simplex virus type 2-infected cells and a potential role in virus assembly. Exp Cell Res 2004;299:486–497.

25. Taylor MP, Burgon TB, Kirkegaard K, et al. Role of microtubules in extracellular release of poliovirus. J Virol 2009;83:6599–6609.

26. Hyde JL, Gillespie LK, Mackenzie JM. Mouse norovirus 1 utilizes the cytoskeleton network to establish localization of the replication complex proximal to the microtubule organizing center. J Virol 2012;86:4110–4122.

27. Xiao PJ, Lentz TB, Samulski RJ. Recombinant adeno-associated virus: Clinical application and development as a gene-therapy vector. Ther Deliv 2012;3:835–856.

28. Wang J, Faust SM, Rabinowitz JE. The next step in gene delivery: Molecular engineering of adeno-associated virus serotypes. J Mol Cell Cardiol 2011;50:793–802.

29. Nonnenmacher M, Weber T. Intracellular transport of recombinant adeno-associated virus vectors. Gene Ther 2012;19:649–658.

30. Xiao PJ, Samulski RJ. Cytoplasmic trafficking, endosomal escape, and perinuclear accumulation of adeno-associated virus type 2 particles are facilitated by microtubule network. J Virol 2012; 86:10462–10473.

31. Grieger JC, Choi VW, Samulski RJ. Production and characterization of adeno-associated viral vectors. Nat Protoc 2006;1:1412–1428.

32. Xiao PJ, Li C, Neumann A, et al. Quantitative 3D tracing of gene-delivery viral vectors in human cells and animal tissues. Mol Ther 2012;20:317–328.

33. Johnson JS, Samulski RJ. Enhancement of adeno-associated virus infection by mobilizing capsids into and out of the nucleolus. J Virol 2009;83:2632–2644.

34. Xiao PJ, Peng ZY, Huang L, et al. Dephosphorylated NSSR1 is induced by androgen in mouse epididymis and phosphorylated NSSR1 is increased during sperm maturation. PLoS One 2011;6:e25667.

35. Vonderheit A, Helenius A. Rab7 associates with early endosomes to mediate sorting and transport of Semliki forest virus to late endosomes. PLoS Biol 2005;3:e233.

36. Nonnenmacher M, Weber T. Adeno-associated virus 2 infection requires endocytosis through the CLIC/GEEC pathway. Cell Host Microbe 2011;10:563–576.

37. Johnson JS, Li C, DiPrimio N, et al. Mutagenesis of adeno-associated virus type 2 capsid protein VP1 uncovers new roles for basic amino acids in trafficking and cell-specific transduction. J Virol 2010;84:8888–8902.

38. Johnson JS, Gentzsch M, Zhang L, et al. AAV exploits subcellular stress associated with inflammation, endoplasmic reticulum expansion, and misfolded proteins in models of cystic fibrosis. PLoS Pathogens 2011;7:e1002053.

39. McDonald D, Vodicka MA, Lucero G, et al. Visualization of the intracellular behavior of HIV in living cells. J Cell Biol 2002;159:441–452.

40. Bailey CJ, Crystal RG, Leopold PL. Association of adenovirus with the microtubule organizing center. J Virol 2003;77:13275–13287.

41. Zhong L, Li B, Jayandharan G, et al. Tyrosine-phosphorylation of AAV2 vectors and its consequences on viral intracellular trafficking and transgene expression. Virology 2008;381:194–202.

42. Grieger JC, Snowdy S, Samulski RJ. Separate basic region motifs within the adeno-associated virus capsid proteins are essential for infectivity and assembly. J Virol 2006;80:5199–5210.

43. Sonntag F, Bleker S, Leuchs B, et al. Adeno-associated virus type 2 capsids with externalized VP1/VP2 trafficking domains are generated prior to passage through the cytoplasm and are maintained until uncoating occurs in the nucleus. J Virol 2006;80:11040–11054.

44. Krendel M, Zenke FT, Bokoch GM. Nucleotide exchange factor GEF-H1 mediates cross-talk be-

tween microtubules and the actin cytoskeleton. Nat Cell Biol 2002;4:294–301.

45. Chang YC, Nalbant P, Birkenfeld J, et al. GEF-H1 couples nocodazole-induced microtubule disassembly to cell contractility via RhoA. Mol Biol Cell 2008;19:2147–2153.

46. Hofmann W, Reichart B, Ewald A, et al. Cofactor requirements for nuclear export of Rev response element (RRE)- and constitutive transport element (CTE)-containing retroviral RNAs. An unexpected role for actin. J Cell Biol 2001;152:895–910.

47. van Loo ND, Fortunati E, Ehlert E, et al. Baculovirus infection of nondividing mammalian cells: Mechanisms of entry and nuclear transport of capsids. J Virol 2001;75:961–970.

48. Minakhina S, Myers R, Druzhinina M, et al. Crosstalk between the actin cytoskeleton and Ran-mediated nuclear transport. BMC Cell Biol 2005;6:32.

49. Broers JL, Ramaekers FC, Bonne G, et al. Nuclear lamins: Laminopathies and their role in premature ageing. Physiol Rev 2006;86:967–1008.

50. Schneider M, Noegel AA, Karakesisoglou I. KASH-domain proteins and the cytoskeletal landscapes of the nuclear envelope. Biochem Soc Trans 2008;36:1368–1372.

51. Hoppe S, Schelhaas M, Jaeger V, et al. Early herpes simplex virus type 1 infection is dependent on regulated Rac1/Cdc42 signalling in epithelial MDCKII cells. J Gen Virol 2006;87:3483–3494.

52. Sharma-Walia N, Naranatt PP, Krishnan HH, et al. Kaposi's sarcoma-associated herpesvirus/human herpesvirus 8 envelope glycoprotein gB induces the integrin-dependent focal adhesion kinase-

Src-phosphatidylinositol 3-kinase-rho GTPase signal pathways and cytoskeletal rearrangements. J Virol 2004;78:4207–4223.

53. Naranatt PP, Krishnan HH, Smith MS, et al. Kaposi's sarcoma-associated herpesvirus modulates microtubule dynamics via RhoA-GTP-diaphanous 2 signaling and utilizes the dynein motors to deliver its DNA to the nucleus. J Virol 2005;79:1191–1206.

54. McGee MD, Rillo R, Anderson AS, et al. UNC-83 IS a KASH protein required for nuclear migration and is recruited to the outer nuclear membrane by a physical interaction with the SUN protein UNC-84. Mol Biol Cell 2006;17:1790–1801.

55. Ketema M, Wilhelmsen K, Kuikman I, et al. Requirements for the localization of nesprin-3 at the nuclear envelope and its interaction with plectin. J Cell Sci 2007;120:3384–3394.

56. Schelhaas M, Ewers H, Rajamäki ML, et al. Human papillomavirus type 16 entry: Retrograde cell surface transport along actin-rich protrusions. PLoS Pathogens 2008;4:e1000148.

57. Fackler OT, Krausslich HG. Interactions of human retroviruses with the host cell cytoskeleton. Curr Opin Microbiol 2006;9:409–415.

58. Greber UF, Way M. A superhighway to virus infection. Cell 2006;124:741–754.

59. Leopold PL, Kreitzer G, Miyazawa N, et al. Dynein- and microtubule-mediated translocation of adenovirus serotype 5 occurs after endosomal lysis. Hum Gene Ther 2000;11:151–165.

60. Suomalainen M, Nakano MY, et al. Microtubule-dependent plus- and minus end-directed motilities

are competing processes for nuclear targeting of adenovirus. J Cell Biol 1999;144:657–672.

61. Suomalainen M, Nakano MY, Boucke K, et al. Adenovirus-activated PKA and p38/MAPK pathways boost microtubule-mediated nuclear targeting of virus. EMBO J 2001;20:1310–1319.

62. Mabit H, Nakano MY, Prank U, et al. Intact microtubules support adenovirus and herpes simplex virus infections. J Virol 2002;76:9962–9971.

63. Ding W, Zhang LN, Yeaman C, et al. rAAV2 traffics through both the late and the recycling endosomes in a dose-dependent fashion. Mol Ther 2006;13:671–682.

64. Kelkar S, De BP, Gao G, et al. A common mechanism for cytoplasmic dynein-dependent microtubule binding shared among adeno-associated virus and adenovirus serotypes. J Virol 2006;80:7781–7785.

65. Lehmann MJ, Sherer NM, Marks CB, et al. Actin- and myosin-driven movement of viruses along filopodia precedes their entry into cells. J Cell Biol 2005;170:317–325.

66. Favoreel HW, Enquist LW, Feierbach B. Actin and Rho GTPases in herpesvirus biology. Trends Microbiol 2007;15:426–433.

67. Ohkawa T, Volkman LE, Welch MD. Actin-based motility drives baculovirus transit to the nucleus and cell surface. J Cell Biol 2010;190:187–195.